minerals

MDPI

Article

Chalcopyrite Leaching in Ferric Sulphate: The Effect of Fe_3O_4-$CuFeS_2$ Galvanic Couple on the Cu Dissolution

Kolela J. Nyembwe [1,2], Elvis Fosso-Kankeu [3,*], Frans Waanders [1], Bhekie B. Mamba [4] and Martin Mkandawire [2]

[1] Water Pollution Monitoring and Remediation Initiatives Research Group, School of Chemical and Minerals Engineering, Faculty of Engineering, North-West University, Potchefstroom 2531, South Africa; djosnyembwe@gmail.com (K.J.N.); frans.waanders@nwu.ac.za (F.W.)
[2] Department of Chemistry, School of Science and Technology, Cape Breton University, Sydney, NS B1P 6L2, Canada; martin_mkandawire@cbu.ca
[3] Department of Metallurgy, Faculty of Engineering and Built Environment, University of Johannesburg, Doornfontein, Johannesburg 2028, South Africa
[4] Institute for Nanotechnology and Water Sustainability (iNanoWS), College of Science Engineering and Technology (CSET), University of South Africa, Florida Science Campus, Johannesburg 1709, South Africa; mambabb@unisa.ac.za
* Correspondence: elvisf@uj.ac.za or elvisfosso.ef@gmail.com

Abstract: Galvanic interactions present alternative strategies to achieve a more efficient Cu dissolution from $CuFeS_2$. The present work studied the interaction between chalcopyrite–magnetite ($CuFeS_2$-Fe_3O_4) in acidified ferric sulphate $Fe_2(SO_4)_3$-H_2SO_4 at a solution pH of 1.8 and a temperature of 25 or 50 °C. The addition of Fe_3O_4 to $CuFeS_2$ forms a galvanic couple, which positively impacts the dissolution of Cu. The results showed that the presence of Fe_3O_4 led to high and fast Cu dissolution rates and decreased significantly the activation energy, from 83 to 57 kJ/mol. In addition to that, the solid residues revealed that $CuFeS_2$ dissolution produced intermediate Cu-S-rich phases: CuS, Cu_2S and Cu_5FeS_4, which appeared to envelop $CuFeS_2$, had no observable intermediate phase while in the presence of Fe_3O_4. The results showed that 94% of Cu could be recovered after 5 h of leaching at 50 °C at a Fe_3O_4/$CuFeS_2$ ratio of 4:1 and a 460 mV Ag/AgCl solution potential. The findings of this study present an option for efficient Cu dissolution from $CuFeS_2$ in ferric sulphate at atmospheric pressure.

Keywords: chalcopyrite; passivation; magnetite; redox potential; ferric sulphate

Citation: Nyembwe, K.J.; Fosso-Kankeu, E.; Waanders, F.; Mamba, B.B.; Mkandawire, M. Chalcopyrite Leaching in Ferric Sulphate: The Effect of Fe_3O_4-$CuFeS_2$ Galvanic Couple on the Cu Dissolution. *Minerals* **2024**, *14*, 162. https://doi.org/10.3390/min14020162

Academic Editor: Jean-François Blais

Received: 28 December 2023
Revised: 25 January 2024
Accepted: 30 January 2024
Published: 2 February 2024

1. Introduction

Copper (Cu) has been used by humans for thousands of years, and its discovery marked a significant milestone in developing the world's civilization. Recently, it has been listed among the critical metals that provide significant contributions towards a more sustainable and low-carbon economy [1]. A major source of Cu is chalcopyrite ($CuFeS_2$), a copper sulphide mineral, which accounts for around 70%–80% of the total global production of Cu. The pyrometallurgy route produces about 85% of the worldwide Cu through a reverberatory furnace or flash smelting. However, the pyrometallurgical treatment appears unattractive for metal extraction due to high sulphur dioxide (SO_2) emission and decreased high-grade mineral ore bodies [2,3]. The hydrometallurgical operation, therefore, seems to promote adequate process economics based on its high metal selectivity and environmental considerations.

The leaching or dissolution process is a vital operation in the hydrometallurgy process. As a result, its efficiency has a major impact on the various downstream processes and, mainly, on the economic and technical aspects of mineral hydrometallurgy. Efficient leaching of chalcopyrite concentrates at ambient pressure still remains a challenge because of the slow dissolution kinetics of this mineral in most leaching media [4,5]. The slow and incomplete dissolution is attributed to forming a passive layer on the mineral surface, regardless

of the method used, whether it is performed via a chemical or bioleaching processes [6,7]. The nature and composition of this barrier remain subject to controversy [8–10]. The most often suggested candidates to form the passivating layers are metal-deficient phases, elemental sulphur and jarosite [11]. In order to enhance the Cu dissolution from the $CuFeS_2$ mineral, different methods and techniques have been proposed from the various laboratory studies. These methods include using a sulphate–chloride solution, microorganisms, fine/ultra-grinding and the addition of silver ions [5,12].

$CuFeS_2$ dissolution could be discussed based on the Ellingham or Eh–pH diagram, which predicts the predominance area of susceptible pieces or phases based on their equilibrium condition for all possible redox reactions (Equations (1)–(4)). The increase of potential on the mineral surface leads to different oxidation reactions, which promote the formation of intermediate phases: bornite (Cu_5FeS_4), covellite (CuS) and chalcocite (CuS_2). According to the Eh–pH diagram, successful copper dissolution from the mineral could be achieved after raising the redox potential above 0.44 V. In addition to that, all intermediate-formed phases are susceptible to dissolving in acidic media at a potential above 0.5 V.

$$CuFeS_2 + 2Fe_2(SO_4)_3 = CuSO_4 + 5FeSO_4 + 2S \quad \Delta G = -16.3 \quad (1)$$

$$5CuFeS_2 + 4Fe_2(SO_4)_3 \rightleftharpoons Cu_5FeS_4 + 12FeSO_4 + 6S \quad \Delta G = -68.7 \quad (2)$$

$$2CuFeS_2 + 2Fe_2(SO_4)_3 \rightleftharpoons Cu_2S + 6FeSO_4 + 3S \quad \Delta G = -30.8 \quad (3)$$

$$CuFeS_2 + Fe_2(SO_4)_3 \rightleftharpoons CuS + 3FeSO_4 + S \quad \Delta G = -18.6 \quad (4)$$

The strategy to overcome passivation and improve metal recovery during the hydrometallurgical treatment of the $CuFeS_2$ mineral is applying and using sulphur-oxidizing microorganisms, which promotes the oxidation of elemental sulphur. The second method, on the other hand, involves galvanic interactions between $CuFeS_2$ and other minerals. These minerals usually have an associated/symbiotic relationship with chalcopyrite and include phases such as pyrite, bornite, magnetite and Arsenopyrite [3]. Due to the difference in the potential between the two minerals, a galvanic effect may occur, making the lower potential phase act as an anode, leading to enhanced oxidation and improved kinetics. The covalent character of most sulphide minerals provides non-localization of charge, resulting in appreciable intrinsic electronic conductivity. FeS_2 is very common in the $CuFeS_2$ mineral ore matrix. Hence, these two phases are in galvanic contact, which leads to the rapid dissolution of Cu from $FeCuS_2$, while FeS_2 is galvanically protected. Particular interest has been given to the galvanic couple $CuFeS_2$-FeS_2, and numerous experimental works [13–16] have been conducted to understand and provide more insight into this alternative route of $CuFeS_2$ dissolution. In the galvanic setup of $CuFeS_2$,-FeS_2 pyrite represents the cathode on which the reduction of the active oxidant in the system takes place while the anode's ($CuFeS_2$) dissolution is significantly enhanced.

The Galvanox^{TM} process makes use of the FeS_2-$CuFeS_2$ galvanic couple [13–15] and reports appreciable results at a Cu recovery of 98% with a FeS_2-to-$CuFeS_2$ (Py:Cp) ratio: roughly 2:1 to 4:1, with the solution potential varying from 440 mV (Ag/AgCl) to 470 mV or higher and the temperature in the range of 70 to 80 °C [17]. The presence of a galvanic couple led to a higher degree of Cu dissolution from $CuFeS_2$ in the presence of FeAsS in an acidic medium culture at a pH of 2 and a temperature of 30 °C [3].

Magnetite (Fe_3O_4) could also be found as an existing impurity in the $CuFeS_2$ ore matrix, especially in the case of carbonatite [18,19]. Being a spinel, the magnetite ($Fe^{2+}Fe^{3+}{}_2O_4$) in an aqueous phase could represent a substantial oxidant source. To the author's knowledge, one recent study reported the existence of galvanic interactions between $CuFeS_2$ and Fe_3O_4 [20]. These interactions might also serve as another alternative for Cu dissolution from the $CuFeS_2$ since oxide minerals are generally more ionic in nature and usually have higher resistivities than sulphide minerals. In addition, the problem with the direct application of the Eh–pH diagram is the possible formation of metastable intermediates, which may be attributed to slow chemical kinetics. However, there is no way to predict

the presence of intermediates from thermodynamics alone. It is, therefore, appropriate to review the kinetic of $CuFeS_2$ in $Fe_2(SO_4)_3$ to better understand the dissolution and phase transition.

Although there have been many studies on mineral additives that can promote the dissolution of chalcopyrite, many types of minerals related to chalcopyrite have not been studied. This work compares the dissolution of Cu from $CuFeS_2$ with and without the addition of Fe_3O_4 in (H_2SO_4-$Fe_2(SO_4)_3$) at a pH value of 1.8, at temperatures of 25 and 50 °C. The study highlights the effect of Fe_3O_4 and evaluates optimum conditions (temperature, potential and $Fe_3O_4/CuFeS_2$ ratio) for maximum Cu dissolution. Lastly, the study reviews intermediate phase conversion and elaborates on the dissolution based on the Cu-S phases.

2. Materials and Methods

2.1. Material

Solutions of the desired pH were prepared using analytical reagent-grade sulphuric acid (H_2SO_4 98% A.C.E.), ferric sulphate ($Fe_3(SO_4)$ • H_2O ACE) and deionized water (<5.0 µs/cm). The redox potential (Ag/AgCl) measurements were determined in reference to the Standard Hydrogen Electrode (SHE).

2.2. Chalcopyrite and Magnetite Sample Characterization

The $CuFeS_2$ sample was obtained as a concentrate from the Phalaborwa Copper Mining Company (Phalaborwa, South Africa). The chalcopyrite sample was dried in an oven at 50 °C for seven days before sub-sampling. Homogenization, in accordance with the soil sampling protocol by the U.S. Environmental Protection Agency [21], was conducted. Approximately 0.5 kg of concentrate was sub-sampled and dried for approximately 20 min at 105 °C. A grain size of less than n 200 microns (<200 µm) was used as a dissolution feed.

The samples were analysed for mineral composition and bulk chemistry using X-ray analysis—X-ray diffraction (XRD) (RigakuUltimaIV with PDXL analysis software (Japan)) and XRF (Rigaku-ZSX Primus II with SQX analysis software (Japan)), respectively. An XRD Rigaku Ultima IV was operated at 40 kV and 30 mA. The Integrated X-ray Powder Diffraction Software (PDXL) (Ver.2.0–2.8.X, Rigaku, Japan) was used for mineral phases, and the instrument's detection limit was 2%. Data were recorded over the range $5° \leq 2\theta \leq 95°$ at a scan rate of 0.5 degrees/min and a step width of 0.01°. The elemental composition (XRF) powder method was carried out on a Rigaku-ZSX Primus II in conjunction with the S.Q.X. analysis software (Rigaku, Japan), operating at 4 kW, 60 kV and 150 mA. The results are illustrated in Figure 1.

2.3. Leaching Media and Tests

$CuFeS_2$ was dissolved in an acidified ferric sulphate solution (H_2SO_4-$Fe_2(SO_4)_3$), with and without Fe_3O_4 addition. A ratio of $Fe_3O_4/CuFeS_2$ varying from 1:1 to 4:1 was used to evaluate the effect of Fe_3O_4 addition on Cu dissolution. The solution was obtained by mixing $Fe_2(SO_4)_3$ with H_2O (water) and H_2SO_4. An initial Fe content (Fe^{3+} = 0.05 MFe) was used for all tests. The media was agitated for 12 h before using it. Dissolution tests were performed at atmospheric conditions at 25 °C or 50 °C. The media pH was measured and maintained at 1.8 with periodic addition of H_2SO_4 (98%). At the same time, the solution oxidation–reduction potential (O.R.P.) was allowed to evolve throughout the dissolution test and was recorded periodically (every 10 min).

Additional dissolution tests were conducted at 50 °C at 400, 430 and 460 mV, and these solution potentials were maintained throughout the dissolution test by periodic addition of hydrogen peroxide in the slurry. This was intended to evaluate the potential dependency of the varying Fe_3O_4-$CuFeS_2$ ratio.

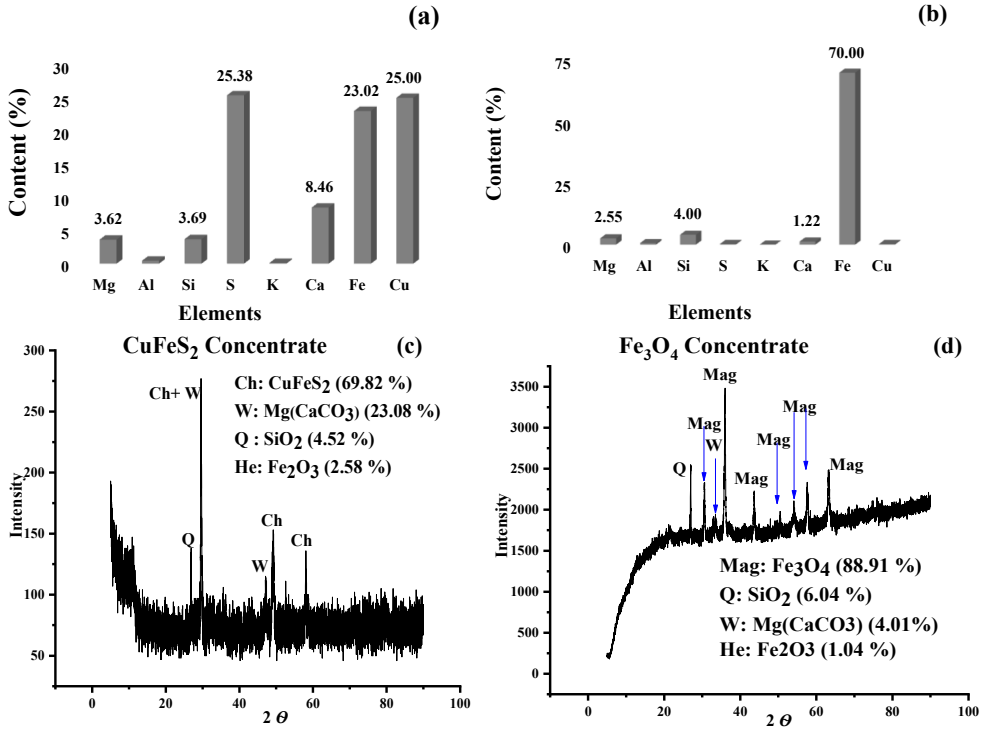

Figure 1. Chemical composition of concentrated $CuFeS_2$ (**a**) and Fe_3O_4 (**b**) samples by XRF; mineralogical composition (**c**,**d**) by XRD.

A pulp density of 10% solid was used in all tests, and kinetic information was obtained by periodic withdrawal (every 20 min) of a 5 mL sample for chemical analysis of total Cu using atomic absorption flame spectrometry (AAFS, Thermo Scientific ICE 3000 series, Cambridge, UK). The redox potential of the leaching solution was measured with a platinum electrode using a saturated Ag/AgCl (3 M KCl) electrode as the reference.

Solid leached residues were analysed for mineral composition using XRD analysis (Rigaku Ultima IV) operating at 40 kV and 30 mA, and PDXL analysis software was used; the instrument's detection limit was 2%. Data were recorded over the range $5° \leq 2\theta \leq 95°$ at a scan rate of 0.5°/min and a step width of 0.01°.

3. Results

3.1. Cu Dissolution Curve and Recovery

All the dissolution curves were asymptotic and characterized by different stages (Figures 2a–c and 3a–c): the first stage (0–60 min) was more rapid than the second stage (60–360 min), and the third stage was the plateau with no Cu dissolution (360–720 min). The rapid stage could be attributed to the fast Cu withdrawal at the mineral surface. At the same time, the second one could correspond to the dissolution of the transient Cu phases formed, which would lead to the third stage with no further dissolution (passivation) [2]. It is worth highlighting that the dissolution conducted without Fe_3O_4 displayed the lowest Cu recovery, as opposed to the mixed $CuFeS_2$-Fe_3O_4 sample, which exhibited high Cu recovery at a much-prolonged first stage.

3.2. Cu Dissolution Recovery at Free O.R.P.

Figure 2 shows the Cu dissolution at free O.R.P. at 25 (Figure 2a) or 50 °C (Figure 2b) for the different samples ($CuFeS_2$ and Fe_3O_4-$CuFeS_2$). Figure 2c,d also show the O.R.P. evolution during the dissolution. At both experimental temperatures (25 and 50 °C), it was observed that the Cu recovery of the mixed sample (Fe_3O_4-$CuFeS_2$) was higher than that of the pure $CuFeS_2$ concentrate sample without added Fe_3O_4. At 25 °C (Figure 2a), only 15% Cu was dissolved from the pure concentrate after 300 min, while 20, 24, 27 and 32%

Cu were observed for the mixed sample (Fe_3O_4-$CuFeS_2$), at a Fe_3O_4/$CuFeS_2$ ratio of 1, 2, 3 and 4, respectively. At 50 °C (Figure 2b), much more Cu was dissolved—47, 51, 57 and 60% Cu were dissolved from the mixed sample, at Fe_3O_4/$CuFeS_2$ ratios of 1, 2, 3 and 4, respectively, while only 21% Cu was dissolved for the pure concentrate ($CuFeS_2$).

A sharp drop (Figure 2c,d) in the solution potential (from 348–336.7 mV) was observed for the $CuFeS_2$ concentrate sample, while all mixed (Fe_3O_4-$CuFeS_2$) sample O.R.P. curves displayed a stagnant/static region at the early stage of the dissolution and dropped thereafter. The rapid drop in solution potential observed for the pure concentrate (without Fe_3O_4 addition) could be due to the rapid consumption of ferric (Fe^{3+}), leading to Cu withdrawal and favouring the formation and increase in Fe^{2+} (Equation (1)). The static region observed for the Fe_3O_4-$CuFeS_2$ sample could be related to the galvanic interaction between $CuFeS_2$ and Fe_3O_4. This stationary state corresponded to the first linear Cu dissolution stage observed on the Cu recovery curve. It could, therefore, be responsible for the high rate and Cu recovery observed for the mixed Fe_3O_4-$CuFeS_2$ sample.

The results from the present investigation show that the Fe_3O_4 addition positively affects the dissolution of $CuFeS_2$ rate and recovery. In addition, the presence of Fe_3O_4 appears to some extent to stabilize the solution O.R.P., since a margin drop-in solution potential is observed in the sample where Fe_3O_4 was absent.

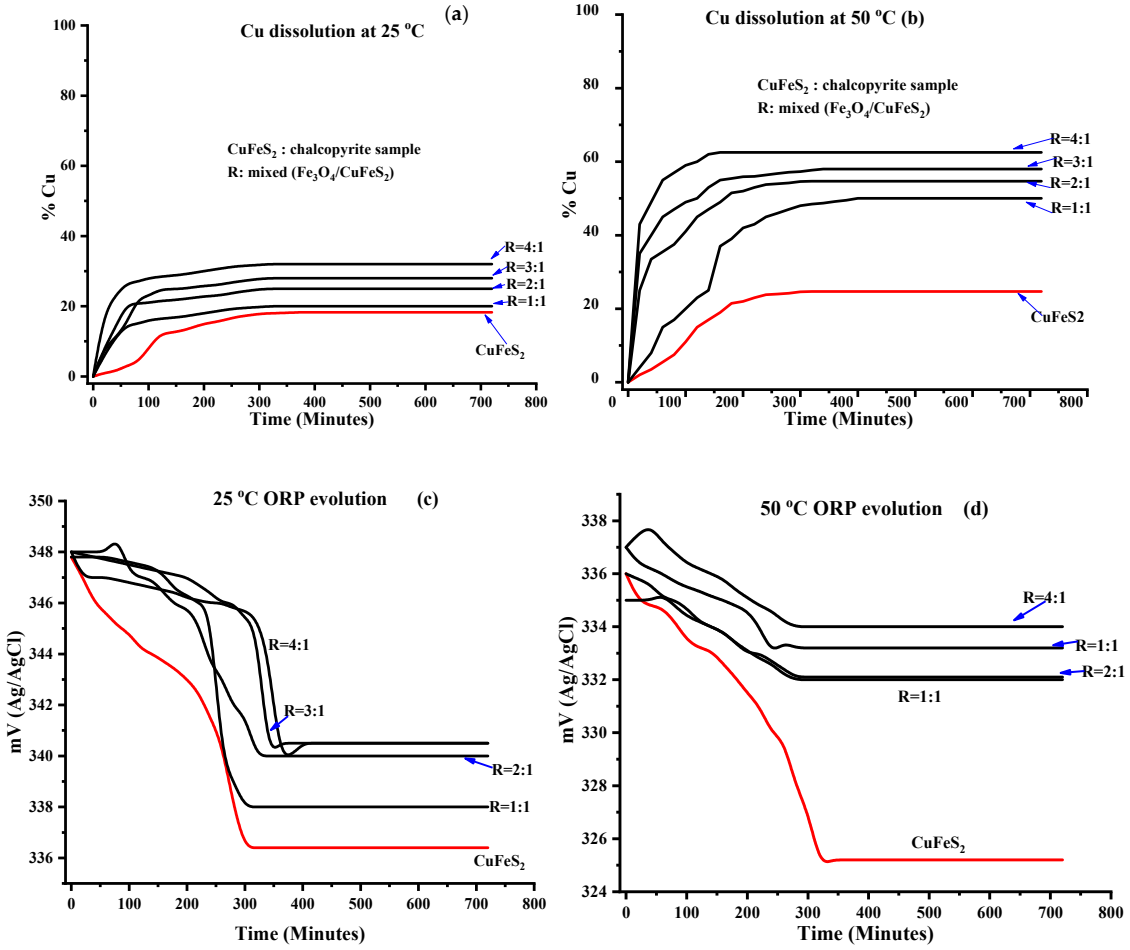

Figure 2. Cu dissolution at uncontrolled O.R.P. and 25 or 50 °C. (**a**) Dissolution at 25 °C at various ratios of magnetite; (**b**) Dissolution 50 °C at various ratios of magnetite; (**c**) Dissolution at 25 °C at various ratios of magnetite; (**d**) Dissolution at 50 °C at various ratios of magnetite.

3.3. Effect of Solution Potential

The effect of potential was evaluated at 50 °C. Figure 3 shows the Cu dissolution at 400, 430 and 460 mV solution potentials. At all solution O.R.P.s (Figure 3a–c), it was observed

that increasing the (Fe_3O_4/$CuFeS_2$) Mag/Ch ratio (from 1:1to 4:1) led to a significant increase in the copper recovery and extraction rate. However, only a smaller difference, between 3:1 and 4:1 (Mag/Ch), was identified. The solution potential appears to play a vital role during the Cu dissolution from the $CuFeS_2$. It was observed that an increase in the solution O.P.R. enhanced the dissolution. More Cu dissolved at 400 mV, much more at 430 and close to complete dissolution was obtained at 460 mV. The present results showed an optimum O.R.P. value of 460 mV, at which 96 and 94% Cu could be achieved after 300 min at a Mag/Ch ratio of 4:1 and 3:1, respectively. These results support previous studies where high Cu recoveries were obtained at low redox potentials) [12,22]. Monitoring and controlling the solution potential appear to be key factors for increasing the dissolution rate in $CuFeS_2$ leaching systems. Most previous work agreed on a narrow potential range of 400–450 mV (Ag | AgCl) where the Cu dissolution yield was at the maximum.

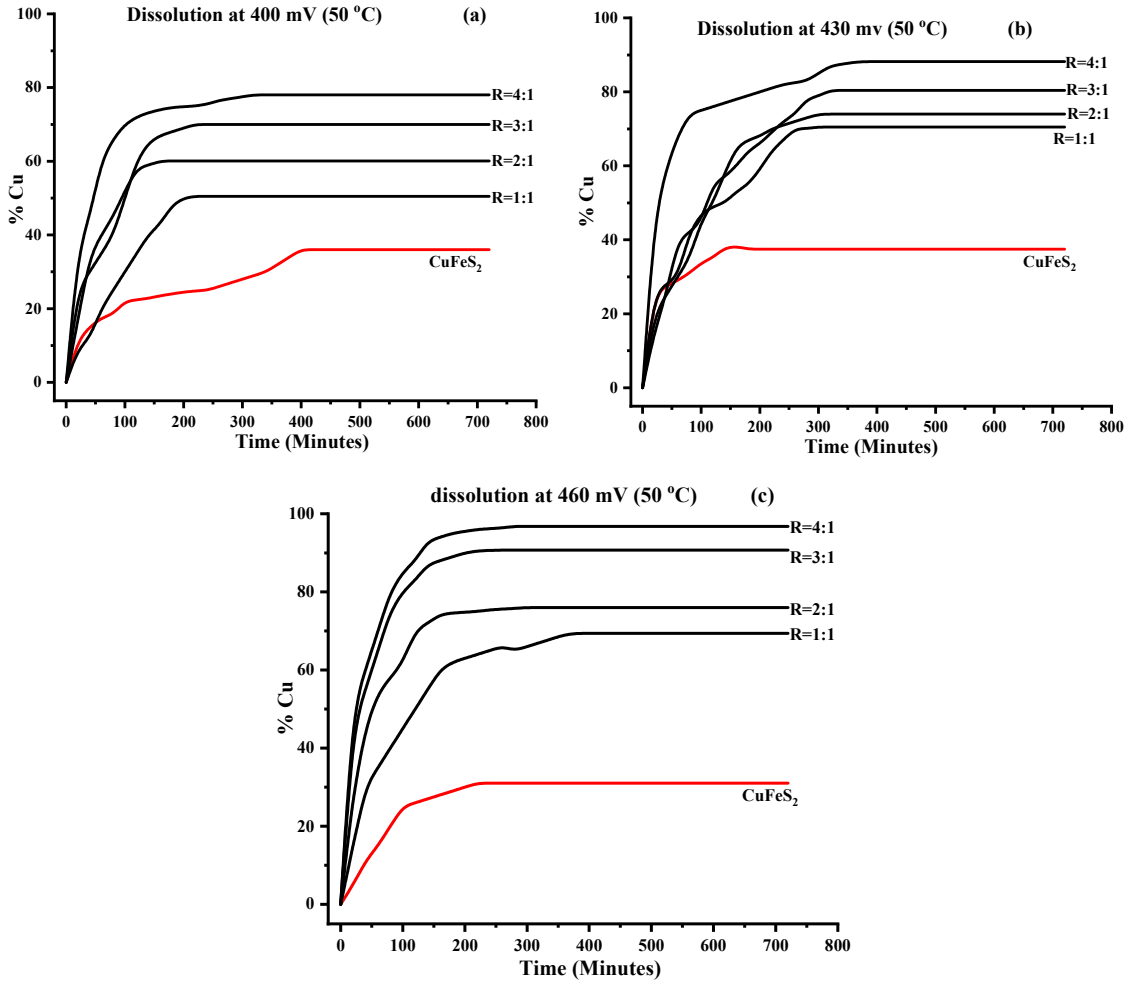

Figure 3. Cu dissolution at controlled O.R.P. (400, 430 or 460 mV Ag/AgCl). (**a**) Dissolution at 400 mV and 50 °C; (**b**) Dissolution at 430 mV and 50 °C; (**c**) Dissolution at 460 mV and 50 °C.

3.4. Effect of Temperature

The temperature was found to affect both the rate and recovery positively. Consequently, its effect was evaluated using the shrinking core model, as shown in Equation (5) when surface chemical reaction controls.

$$1 - (1 - a)^{1/3} = k' \cdot t \quad (5)$$

where a is the copper ion concentration, k′ corresponds to the reaction rate constant and t means the leaching time. The Arrhenius equation (i.e., Equation (6)) was used to calculate the activation energy of chalcopyrite leaching:

$$k' = Ae^{-(Ea/RT)} \quad (6)$$

where A is the pre-exponential factor, Ea is the activation energy ($J \cdot mol^{-1}$), R is the universal gas constant ($J \cdot mol^{-1} \cdot K^{-1}$) and T is the absolute temperature in Kelvin (K). Figure 4a shows the fitting of the lnk′ against 1/T (Arenhius plot) according to the Cu extraction data collected, and Figure 4b shows the effect of Fe_3O_4 addition on the $CuFeS_2$ Ea values.

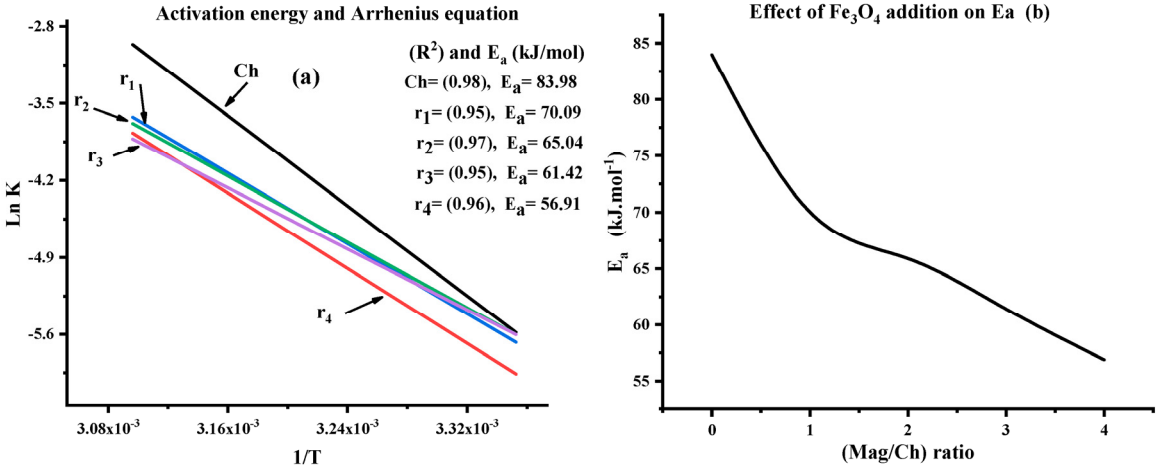

Figure 4. Arrhenius plot at various $Fe_3O_4/CuFeS_2$ ratios (**a**) and effect of Fe_3O_4 addition on the activation energy (**b**).

The $CuFeS_2$ concentrate sample dissolution had the highest Ea (around 80 kJ/mol). Its high value was consistent with the literature values [23]. The activation energy decreased with the addition of Fe_3O_4 (Figure 4b). At a $Fe_3O_4/CuFeS_2$ ratio of 1:1, the Ea value was 70 $kJ \cdot mol^{-1}$. This value went down to 65 when the Fe_3O_4 content was double ($Fe_3O_4/CuFeS_2$ = 2) and decreased further to 61 $kJ \cdot mol^{-1}$ and 56 $kJ \cdot mol^{-1}$ when the $Fe_3O_4/CuFeS_2$ ratio increased respectively to 3 and 4. The decrease in the Ea value with the addition of Fe_3O_4 could suggest that the dissolution process of $CuFeS_2$ becomes much easier in the presence of Fe_3O_4. Although the Ea value substantially decreased from 84 to 56 $kJ \cdot mol^{-1}$, all the Ea values were above 40 $kJ \cdot mol^{-1}$, implying that all dissolution was controlled by the same process. The dissolution process was chemically controlled at the mineral surface [24].

3.5. Solid Residue Analysis

Figure 5 summarises the mineralogical composition of the solid residues at 50 °C and 460 mV. Figure 5a displays the residue mineral content of the $CuFeS_2$ without adding Fe_3O_4, while Figure 5b presents the mineral phase of the mixed Fe_3O_4-$CuFeS_2$ at a Mag/Ch ratio of 4:1.

In both cases, the $CuFeS_2$ main peaks (2 theta = 29.46, 48.93 and 57.95) appeared to decrease in intensity compared to the feed sample. The dissolution of $CuFeS_2$ without Fe_3O_4 (Figure 5a) displayed the presence of a Cu-rich phase (bornite (Bo), chalcocite (Cx) and covellite (Co)). The presence of these Cu-rich intermediates appeared to support earlier investigation [25], which underlined the preferential dissolution of Fe over Cu, leading to the formation of a Fe-deficient chalcopyrite mineral (defect chalcopyrite structure Cu1-xFe1-yS2-z) to which the present identified species could be a part.

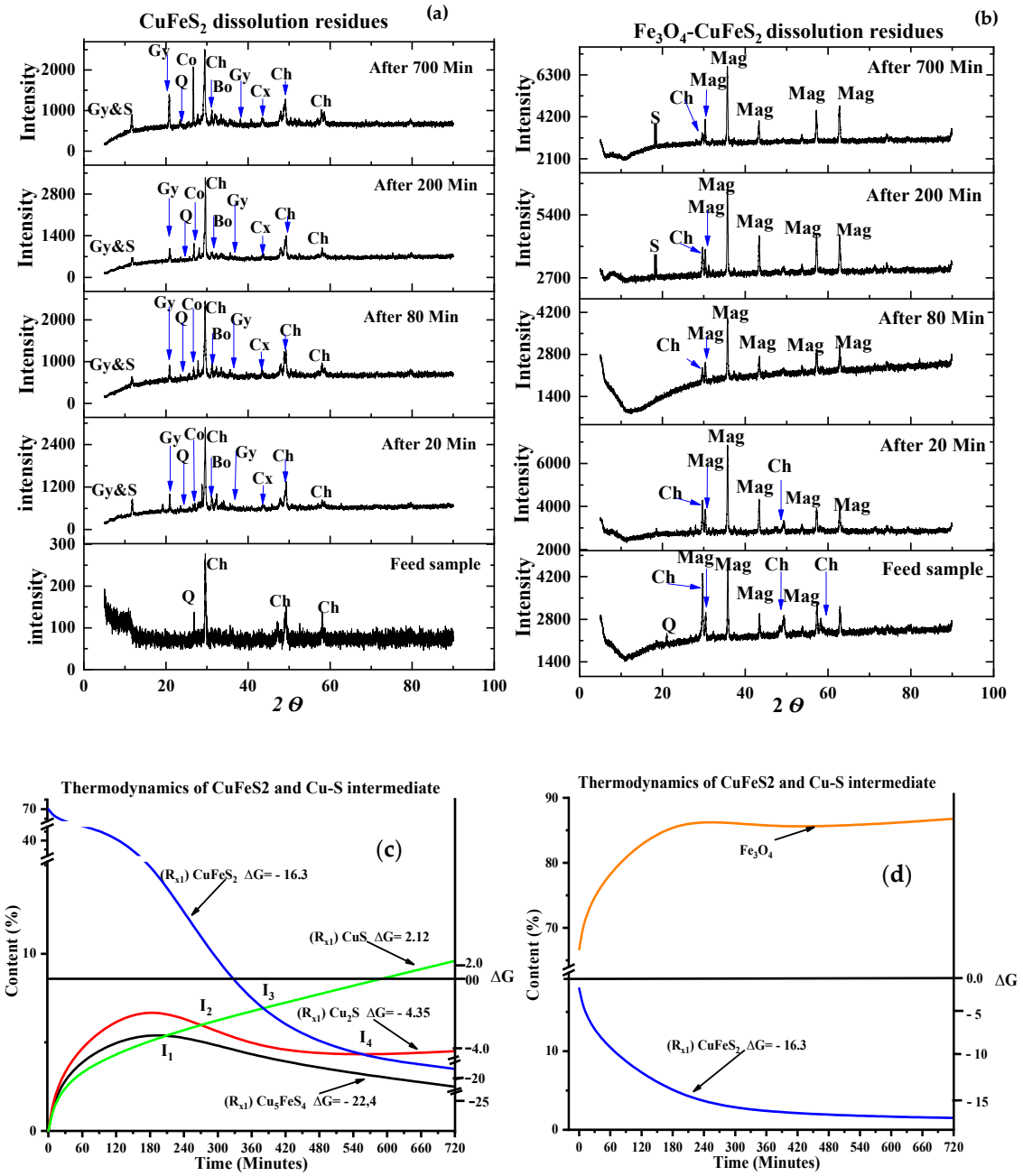

Figure 5. XRD analysis of $CuFeS_2$ (**a**) and Fe_3O_4/$CuFeS_2$ ratio of 4:1 (**b**); thermodynamic analysis of $CuFeS_2$ Cu-S intermediate phase dissolution (**c**) Intermediate phases; (**d**) Fe_3O_4 and $CuFeS_2$ trends.

On the other hand, the mixed Fe_3O_4-$CuFeS_2$ sample residues remained dominated by the Fe_3O_4 (Figure 5b), and the Fe_3O_4 content increased due to the $CuFeS_2$ dissolution. These results showed that the Fe_3O_4 content increased from 66.4% in the feed sample (Mag/Ch = 4:1) to 86.2% after 5 h of dissolution (Figure 5d). This supports the presence of the galvanic couple between $CuFeS_2$ and Fe_3O_4, as $CuFeS_2$ dissolves more rapidly, while Fe_3O_4 becomes galvanically protected. This finding also confirms that most of the Fe_3O_4 could be recycled if the process is used. In addition to that, the Fe_3O_4-$CuFeS_2$ mixed residue sample did not reveal the presence of any intermediate phase. This could suggest that the dissolution of Cu from the $CuFeS_2$ sample takes place by mineral phase intermediates. In contrast, no intermediate phase is formed in galvanic interaction, and the Cu dissolves directly from $CuFeS_2$, according to Equation (1).

Thermodynamically, bornite is the most favourable phase to be formed (Equation (2)), followed by chalcocite (Equation (3)) and, lastly, covellite (Equation (4)). These Cu-S phases could react further into new Cu-S-richer phases or leach to promote Cu recovery. CuS is more likely to form from Cu_5FeS_4 (Equation (5)) than Cu_2S (Equation (6)). Similarly, [26,27] also reported the presence of CuS due to a transient species during the ferric leaching of Cu_5FeS_4. The intersection points in Figure 5c between the various intermediate phases could suggest, on the one hand, the dissolution competition between phases. On the other hand, it could suggest the transformation from one phase into the other. In that sense, I1, I2 and I3 observed between CuS/Cu_5FeS_4, CuS/Cu_2S and $CuS/CuFeS_2$ suggest the competition between both dissolution reactions and, since CuS is refractory, Cu_5FeS_4, Cu_2S and $CuFeS_2$ dissolve by transformation into CuS according to Equations (7)–(9). This explains the increase in the CuS content (Figure 5a) and its cumulative behaviour (Equation (11)), as observed in the XRD analysis. Meanwhile, I4 strictly represents the direct conversion of $CuFeS_2$ to Cu_2S without any Cu^{2+} withdrawal, according to Equation (11).

$$Cu_5FeS_4 + Fe_2(SO_4)_3 \rightleftharpoons 4CuS + 3FeSO_4 + Cu^{2+} \quad \Delta G = -22.4 \quad (7)$$

$$Cu_2S + Fe_2(SO_4)_3 \rightleftharpoons CuS + 2FeSO_4 + Cu^{2+} \quad \Delta G = -4.35 \quad (8)$$

$$CuFeS_2 + Fe_2(SO_4)_3 \rightleftharpoons CuS + 3FeSO_4 + S \quad \Delta G = -18.6 \quad (9)$$

$$CuS + Fe_2(SO_4)_3 \rightleftharpoons 2FeSO_4 + S_0 + Cu^{2+} \quad \Delta G = 2.12 \quad (10)$$

$$2CuFeS_2 + 2Fe_2(SO_4)_3 \rightleftharpoons Cu_2S + 6FeSO_4 + 3S \quad \Delta G = -30.8 \quad (11)$$

4. Conclusions

This work investigated the dissolution of $CuFeS_2$ in acidic $Fe_2(SO_4)_3$ in the presence of Fe_3O_4. The results show the positive impact of Fe_3O_4 on Cu dissolution from $CuFeS_2$. It was observed that Fe_3O_4 enhanced the Cu dissolution, which was highly correlated to temperature. The results showed that 94% of Cu could be recovered after 5 h at 50 °C at a $Fe_3O_4/CuFeS_2$ ratio of 4:1. The activation energy considerably decreased in the presence of Fe_3O_4. It was found to be 57 kJ/mol, suggesting a chemically controlled process through surface reaction. The solid residues revealed that $CuFeS_2$ dissolution produced intermediate Cu-rich phases: CuS, Cu_2S and Cu_5FeS_4, which appeared to envelop $CuFeS_2$, while in the presence of Fe_3O_4, no intermediate phase was observed. The findings of this study present an option for efficient Cu dissolution from $CuFeS_2$ in ferric sulphate.

5. Patents

Data from this work have been used to claim the novelty of the work, and a patent was granted in 2022.

Author Contributions: Conceptualization, E.F.-K. and K.J.N.; methodology, E.F.-K. and K.J.N.; software, E.F.-K., B.B.M. and K.J.N.; validation, M.M., B.B.M., F.W. and E.F.-K.; formal analysis, K.J.N.; investigation, K.J.N., E.F.-K. and M.M.; resources, E.F.-K., F.W. and M.M.; data curation, K.J.N.; writing—original draft preparation, K.J.N.; writing—review and editing, M.M.; visualization, K.J.N.; supervision, E.F.-K. and M.M.; project administration, E.F.-K. and F.W.; funding acquisition, E.F.-K. and M.M. All authors have read and agreed to the published version of the manuscript.

Funding: The authors are thankful to the North-West University (IREA 2020) and the University of South Africa (MIN/21) for the financial support and promotion of this research.

Data Availability Statement: The data presented in this study are available on request from the corresponding author. The data are not publicly available due to privacy.

Acknowledgments: The authors are thankful to the local South African mining company that participated in this research by providing the samples to the extraction metallurgy laboratory at the University of Johannesburg for equipment utilization.

Conflicts of Interest: The authors declare no conflicts of interest.

References

1. Seck, G.S.; Hache, E.; Bonnet, C.; Simoën, M.; Carcanague, S. Copper at the crossroads: Assessment of the interactions between low-carbon energy transition and supply limitations. *Resour. Conserv. Recycl.* **2020**, *163*, 105072. [CrossRef] [PubMed]
2. Nyembwe, K.J.; Fosso-Kankeu, E.; Waanders, F.; Mkandawire, M. Iron-Speciation Control of Chalcopyrite Dissolution from a Carbonatite Derived Concentrate with Acidic Ferric Sulphate Media. *Minerals* **2021**, *11*, 963. [CrossRef]
3. Shangguan, X.; Liu, Y.; Liu, R.; Wang, K.; Belqadi, W.; He, J.; Tong, Y.; Shen, L.; Zeng, W.; Wu, X.; et al. Enhanced Chalcopyrite Dissolution in Acidic Culture Medium: The Impact of Arsenopyrite Presence. *Minerals* **2024**, *14*, 50. [CrossRef]
4. Zhong, S.; Li, Y. An improved understanding of chalcopyrite leaching kinetics and mechanisms in the presence of NaCl. *J. Mater. Res. Technol.* **2019**, *8*, 3487–3494. [CrossRef]
5. Ruiz, M.C.; Montes, K.S.; Padilla, R. Galvanic effect of pyrite on chalcopyrite leaching in sulfate-chloride media. *Miner. Process. Extr. Met. Rev.* **2014**, *36*, 65–70. [CrossRef]
6. Watling, H. Chalcopyrite hydrometallurgy at atmospheric pressure: 1. Review of acidic sulfate, sulfate–chloride and sulfate–nitrate process options. *Hydrometallurgy* **2013**, *140*, 163–180. [CrossRef]
7. Xiong, X.; Hua, X.; Zheng, Y.; Lu, X.; Li, S.; Cheng, H.; Xu, Q. Oxidation mechanism of chalcopyrite revealed by X-ray photoelectron spectroscopy and first principles studies. *Appl. Surf. Sci.* **2018**, *427*, 233–241. [CrossRef]
8. Tshilombo, A.F. Mechanism and Kinetics of Chalcopyrite Passivation and Depassivation during Ferric and Microbial Leaching. British Columbia. 2004. Available online: https://open.library.ubc.ca/collections/831/items/1.0078957 (accessed on 23 April 2018).
9. Naderi, H.; Abdollahy, M.; Mostoufi, N.; Koleini, M.J.; Shojaosadati, S.A.; Manafi, Z. Kinetics of chemical leaching of chalcopyrite from low grade copper ore: Behavior of different size fractions. *Int. J. Miner. Met. Mater.* **2011**, *18*, 638–645. [CrossRef]
10. Olvera, O.; Rebolledo, M.; Asselin, E. Atmospheric ferric sulfate leaching of chalcopyrite: Thermodynamics, kinetics and electrochemistry. *Hydrometallurgy* **2016**, *165*, 148–158. [CrossRef]
11. Klauber, C. A critical review of the surface chemistry of acidic ferric sulphate dissolution of chalcopyrite with regards to hindered dissolution. *Int. J. Miner. Process.* **2008**, *86*, 1–17. [CrossRef]
12. Koleini, S.J.; Aghazadeh, V.; Sandström, Å. Acidic sulphate leaching of chalcopyrite concentrates in presence of pyrite. *Miner. Eng.* **2011**, *24*, 381–386. [CrossRef]
13. Dixon, D.; Mayne, D.; Baxter, K. Galvanox^{TM}-A novel galvanically-assisted atmospheric leaching technology for copper concentrates. *Can. Met. Q.* **2008**, *47*, 327–336. [CrossRef]
14. Koleini, S.M.J.; Jafarian, M.; Abdollahy, M.; Aghazadeh, V. Galvanic leaching of chalcopyrite in atmospheric pressure and sulfate media: Kinetic and surface studies. *Ind. Eng. Chem. Res.* **2010**, *49*, 5997–6002. [CrossRef]
15. Majuste, D.; Ciminelli, V.; Osseo-Asare, K.; Dantas, M. Quantitative assessment of the effect of pyrite inclusions on chalcopyrite electrochemistry under oxidizing conditions. *Hydrometallurgy* **2012**, *113-114*, 167–176. [CrossRef]
16. Payant, R.; Rosenblum, F.; Nesset, J.; Finch, J. The self-heating of sulfides: Galvanic effects. *Miner. Eng.* **2012**, *26*, 57–63. [CrossRef]
17. Salehi, S.; Noaparast, M.; Shafaie, S.Z. Kinetics of chalcopyrite galvanic leaching using sulfate medium at low temperature in the Galvanox TM process. *Int. J. Min. Geo-Eng.* **2016**, *50*, 157–161. [CrossRef]
18. Makvandi, S.; Beaudoin, G.; McClenaghan, B.M.; Layton-Matthews, D. The surface texture and morphology of magnetite from the Izok Lake volcanogenic massive sulfide deposit and local glacial sediments, Nunavut, Canada: Application to mineral exploration. *J. Geochem. Explor.* **2015**, *150*, 84–103. [CrossRef]
19. Nyembwe, K.J.; Fosso-Kankeu, E.; Waanders, F.; Nyembwe, K.D. Structural, compositional and mineralogical characterization of carbonatitic copper sulfide: Run of mine, concentrate and tailings. *Int. J. Miner. Met. Mater.* **2019**, *26*, 143–151. [CrossRef]
20. Saavedra, A.; García-Meza, J.V.; Cortón, E.; González, I. Understanding galvanic interactions between chalcopyrite and magnetite in acid medium to improve copper (Bio)Leaching. *Electrochim. Acta* **2018**, *265*, 569–576. [CrossRef]
21. Simons, K. *Soil Sampling*; U.S. Environmental Protection Agency Laboratory Services & Applied Science Division: Athens, GA, USA, 2014.
22. Sandström, A.; Shchukarev, A.; Paul, J. XPS characterisation of chalcopyrite chemically and bio-leached at high and low redox potential. *Miner. Eng.* **2005**, *18*, 505–515. [CrossRef]
23. Debernardi, G.; Carlesi, C. Chemical-electrochemical approaches to the study passivation of chalcopyrite. *Miner. Process. Extr. Met. Rev.* **2013**, *34*, 10–41. [CrossRef]
24. Crundwell, F. The dissolution and leaching of minerals: Mechanisms, myths and misunderstandings. *Hydrometallurgy* **2013**, *139*, 132–148. [CrossRef]
25. Acero, P.; Cama, J.; Ayora, C.; Asta, M.P. Chalcopyrite dissolution rate law from pH 1 to 3. *Geol. Acta* **2009**, *7*, 389–397. [CrossRef]
26. Dutrizac, J.E.; Chen, T.T.; Jambor, J.L. Mineralogical changes occurring during the ferric lon leaching of bornite. *Met. Trans. B* **1985**, *16*, 679–693. [CrossRef]
27. Zhao, H.-B.; Hu, M.-H.; Li, Y.-N.; Zhu, S.; Qin, W.-Q.; Qiu, G.-Z.; Wang, J. Comparison of electrochemical dissolution of chalcopyrite and bornite in acid culture medium. *Trans. Nonferrous Met. Soc. China* **2015**, *25*, 303–313. [CrossRef]